PAPER

Mechanisms of thermoelectric efficiency enhancement in Lu-doped Bi_2Te_3

To cite this article: Oleg Ivanov and Maxim Yaprintsev 2018 *Mater. Res. Express* **5** 015905

View the article online for updates and enhancements.

Materials Research Express

PAPER

Mechanisms of thermoelectric efficiency enhancement in Lu-doped Bi$_2$Te$_3$

Oleg Ivanov [ORCID] and Maxim Yaprintsev

Belgorod State University, Pobedy 85, 394015, Russia

E-mail: Ivanov.Oleg@bsu.edu.ru

Abstract

The Lu$_x$Bi$_{2-x}$Te$_3$ thermoelectrics with $x = 0, 0.05, 0.1$ and 0.2 have been prepared by microwave-solvothermal method and spark plasma sintering. All the compositions are semiconductors of n-type conductivity. It was found that electron concentration increases and electron mobility decreases with x increasing. The Lu doping results in remarkable increase of the thermoelectric figure-of-merit from $\sim$0.4 for undoped Bi$_2$Te$_3$ up to $\sim$0.9 for Bi$_{1.9}$Lu$_{0.1}$Te$_3$. Enhancing the thermoelectric efficiency at the doping is originated from: (i) increase of the electron concentration since the Lu atoms behave as donors in the Bi$_2$Te$_3$ lattice that decreases the specific electrical resistance, (ii) increase of the Seebeck coefficient via increase of the density-of-states effective mass for conduction band, (iii) decrease of the total thermal conductivity via forming the point defects like antisite defects and Lu atoms substituting for the Bi sites. Formation of narrow non-parabolic impurity band lying near the Fermi energy with sharp density of states is believed to be responsible for increasing the density-of-states effective mass and decreasing the electron contribution to the total thermal conductivity.

Introduction

Thermoelectric materials convert the waste heat energy into the electrical energy and are ones of the promising candidates for clean and environmental friendly energy technologies [1]. Thermoelectric efficiency of materials is characterized by the dimensionless figure-of-merit coefficient, ZT, expressed as $(S^2/\rho k)T$, where T is the absolute temperature, S is the Seebeck coefficient, ρ is the specific electrical resistance, and k is the thermal conductivity [2]. So, the lower k and ρ, and higher S values should be combined in material to reach the higher ZT value. Unfortunately, the thermoelectric efficiency of most materials remained too low until now ($ZT \approx 1$). Therefore, the thermoelectric materials are often too inefficient to be cost-effective in most applications. A number of investigations using various physical and technological approaches have been carried out to enhance the performance of the thermoelectric materials [3–11].

At present, Bi$_2$Te$_3$ and Bi$_2$Te$_3$-based compounds are known to be the best materials for various thermoelectric applications around room temperature [12–14]. An element doping is one of obvious and promising ways to get an optimal combination of the S, ρ and k values resulting in the ZT enhancement in the Bi$_2$Te$_3$-based compounds [15–20]. Recently it was found that rare earth elements, R, (R = Lu, Ce, Sm, Er, La, etc) can be used as dopants to remarkably enhance the thermoelectric performance of Bi$_2$Te$_3$ [21–28]. There are several effects of the R doping on the thermoelectric properties of Bi$_2$Te$_3$ as follows: (a) increase of carrier concentration due to donor-like effects at rare earth elements substituting for Bi site in the Bi$_2$Te$_3$ lattice; (b) increase of electron and phonon scattering by various point defects forming in the crystal lattice at the doping; (c) formation of narrow non-parabolic impurity band with high density of states near the Fermi level effecting on both the Seebeck coefficient and thermal conductivity. Mechanisms of these effects could be extracted from a detailed examination of the ρ, S and k behaviour for R-doped Bi$_2$Te$_3$ within a broad temperature range and at various R content.

The aim of this paper is to find the mechanisms of the thermoelectric efficiency enhancement in the Lu$_x$Bi$_{2-x}$Te$_3$ compounds with $x = 0, 0.05, 0.1$ and 0.2.

Figure 1. XRD patterns of $Lu_xBi_{2-x}Te_3$ with $x = 0$ (a), 0.05 (b), 0.1 (c) and 0.2 (d).
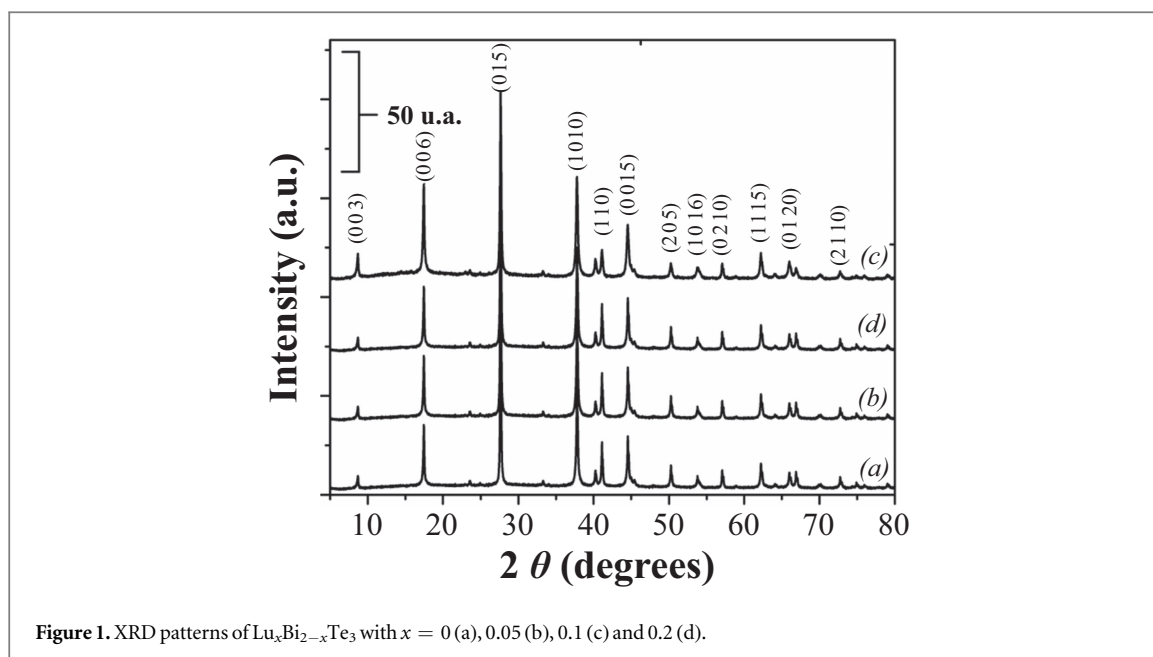
Methods

Microwave-solvothermal synthesis was applied to prepare the starting powders of the compositions with various Lu content. Analytically pure chemicals were used for the synthesis (bismuth oxide, Bi_2O_3, tellurium oxide, TeO_2, lutetium oxide, Lu_2O_3, ethylene glycol, nitric acid and N,N-dimethylformamide). The Bi_2O_3, TeO_2 and Lu_2O_3 oxides taken in a stoichiometric ratio for each composition were dissolving in mixture of concentrated nitric acid and ethylene glycol. Then N,N-dimethylformamide was added in mixture after dissolving. The microwave-assisted reaction was carried out in a MARS-6 microwave reactor with power of 1000 W at 2.45 MHz working frequency. The synthesis was carried out for 15 min at temperature of 463 K and pressure of 40 bars. Spark plasma sintering method by using a SPS-25/10 system was applied to sinter bulk materials at pressure of 40 MPa, temperature of 683 K and sintering time 5 min.

The specific electrical resistance and Seebeck coefficient were measured by using a ZEM-3 system. A TC-1200 system was applied to determine the thermal conductivity by the laser flash method. The ρ, S and k values were measured within the temperature range from 295 K up to 630 K. The maximum temperature of this range is much lower as compared to the melting point of Bi_2Te_3 equal to 858 K. Besides, the SPS temperature was equal to 683 K that is also higher than maximum temperature used to measure the transport parameters. Within the 295–630 K range Lu-doped Bi_2Te_3 demonstrated the thermal stability enough to get reproducible results of measurements. Choosing a broad temperature range for the transport parameters measurements allowed us to study changes in the thermoelectric properties of Lu-doped Bi_2Te_3 induced by intrinsic conductivity onset.

The type, concentration, n, and Hall mobility, μ_H, of the majority charge carriers were extracted from the Hall effect study carried out by a Cryogenic Free system.

To determine a phase composition of the $Lu_xBi_{2-x}Te_3$ compounds with $x = 0$, 0.05, 0.1 and 0.2, x-ray diffraction (XRD) analysis was performed by a Rigaku Ultima IV diffractometer with CuK_α-radiation. XRD patterns are shown in figure 1.

All the diffraction peaks can be indexed to the rhombohedral Bi_2Te_3 with space $\boldsymbol{R\bar{3}m}$ symmetry (standard JCPDS 15-0863 card) and no remarkable impure phases such as tellurium, bismuth, lutetium or their other compounds are observed. There is a small difference between the ionic radii of Lu (1.001 Å) and bismuth (1.100 Å) [29]. So, the Lu substitution effect on lattice parameters of Bi_2Te_3 would be too small to be founded in XRD phase.

Important question is whether Lu really substitutes for Bi site in the Bi_2Te_3 lattice? There are a few evidences and reasons to believe so. First of all, in addition to very close ionic radii, the Bi and Te atoms have the same valence equal to 3+. Second, to determine a correct elemental composition of materials prepared, a Shimadzu ICP (Inductively Coupled Plasma) emission spectrometer ICPE-9000 was applied. As wastage and volatilization are unavoidable during spark plasma sintering, the real composition may deviate from the nominal one. However, according to analysis results, a content of various elements really corresponds to the compositions with $x = 0$, 0.05, 0.1 and 0.2 (table 1). Moreover, the atomic (Bi+Lu)/Te ratio is equal to 2/3 for all compositions. Next, for the composition with $x = 0$ the Lu content is large enough to observe any traces of

Table 1. The content of elements versus composition.

| x	Bi, at%	Te, at%	Lu, at%
0.00	40.13	59.87	–
0.05	39.07	59.92	1.01
0.10	38.07	59.95	1.98
0.20	36.03	59.98	3.99

impurity Lu phases by the XRD method. But, no impurity phases were found for this composition. Finally, the paramagnetic resonance absorption spectra of the $Gd_xBi_{2-x}Te_3$ alloys were earlier measured at room temperature [30]. These data showed that Gd^{3+} site has a C_{3v} symmetry, indicating a true substitution of Bi atoms by Gd. Taking into account, that rare earth elements have very close properties, Lu should behave in the same manner as Gd at the Bi_2Te_3 doping, that is Lu would substitute for Bi site.

Results and discussion

The type, concentration and Hall mobility of the majority charge carriers

According to the Hall effect study, the majority charge carriers for all Lu-doped compounds are electrons. It is known [18–20] that the type and carrier concentration in Bi_2Te_3 are closely related to various point defects. The most common defects are vacancies at Te sites (positively charged $V_{Te}^{\cdot\cdot}$, providing two electrons, e' per defect), vacancies at Bi sites (negatively charged V_{Bi}''', contributing three holes per defect) and antisite defects of Bi at Te sites (negatively charged Bi_{Te}', accompanied with formation of one hole, $h^{\cdot}$).

The energy of evaporation for Te ($52.55\ kJ\ mol^{-1}$) is much lower as compared to Bi ($104.80\ kJ\ mol^{-1}$). So, the evaporation of Te is much easier than that of Bi. Each $V_{Te}^{\cdot\cdot}$ vacancy leaves two free electrons in accordance with equation (1)

$$Bi_2Te_3 = 2Bi_{Bi}^{\times} + 2Te_{Te}^{\times} + Te(g) + V_{Te}^{\cdot\cdot} + 2e', \tag{1}$$
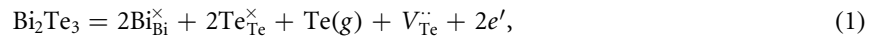
where symbol g is corresponding to a gaseous phase.

A ratio of V_{Bi}''' and $V_{Te}^{\cdot\cdot}$ vacancies are always equal to 2:3 resulting in a zero net free charge, as shown in equation (2)

$$5Bi_2Te_3 = 8Bi_{Bi}^{\times} + 10Te_{Te}^{\times} + 5Te(g) + (2V_{Bi}''' + 3V_{Te}^{\cdot\cdot}) + 2Bi_{Te}' + 2h^{\cdot} \tag{2}$$
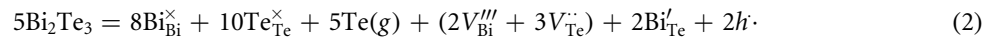
Due to a small difference in electronegativity between Te and Bi, antisite defects are induced since Bi can easily jump from Bi sites to Te sites contributing one hole as a free carrier (equation (2)).

Besides, for polycrystalline Bi_2Te_3, the dangling bonds at grain boundaries due to Te deficiencies can also be considered as fractional-$V_{Te}^{\cdot\cdot}$ acting as n-type dopants in the same manner as whole-$V_{Te}^{\cdot\cdot}$ defects inside the grains. Therefore, most polycrystalline Bi_2Te_3 samples are n-type semiconductors. For the polycrystalline samples prepared by the deformation methods such as ball milling, hot pressing and spark plasma sintering, the deformation induced donor-like effect can also take place. A deformation can induce a non-basal slip and produces, on average, 3 Te to 2 Bi vacancy-interstitial pairs [19]. When abundant Bi vacancies are created, Bi atoms occupying Te sites would more readily diffuse back into its original sublattices and excess Te vacancies are produced in accordance with equation (3)

$$2V_{Bi}''' + 3V_{Te}^{\cdot\cdot} + Bi_{Te}^{\cdot\cdot} = V_{Bi}''' + Bi_{Bi}^{\times} + 4V_{Te}^{\cdot\cdot} + 6e'. \tag{3}$$
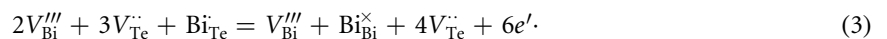
Six excess electrons are generated per equation as an additional source of electrons.

Thus, both $V_{Te}^{\cdot\cdot}$ vacancies (equation (1)) and deformation induced donor-like effect (equation (3)) will generate electrons as the majority charge carriers in $Lu_xBi_{2-x}Te_3$.

The concentration and Hall mobility values of electrons for these compositions taken at room temperature are collected in table 2.

So, the Lu doping results in increase of n and decrease of μ_H. The doping effect on n is usually attributed to the difference of electronegativity for elements forming the antisite Bi_{Te}' defects responsible for holes generation in Bi_2Te_3 (equation (2)). The electronegativity values are equal to 2.1, 2.02 and 1.27 for Te, Bi and Lu, respectively. So, the larger electronegative difference for Lu–Te pair compared to Bi–Te pair will decrease the concentration of antisite defects at Te-sites which contributes one hole per defect and hence results in more electrons.

Table 2. The concentration, Hall mobility and density-of-state effective mass of the majority charge carriers versus composition.

x	n, 10^{19}, cm^{-3}	μ_H, cm^2 V^{-1} s^{-1}	m^*
0.00	1.2	420	$0.11 m_0$
0.05	1.3	385	$0.15 m_0$
0.10	2.4	360	$0.17 m_0$
0.20	4.1	150	$0.25 m_0$
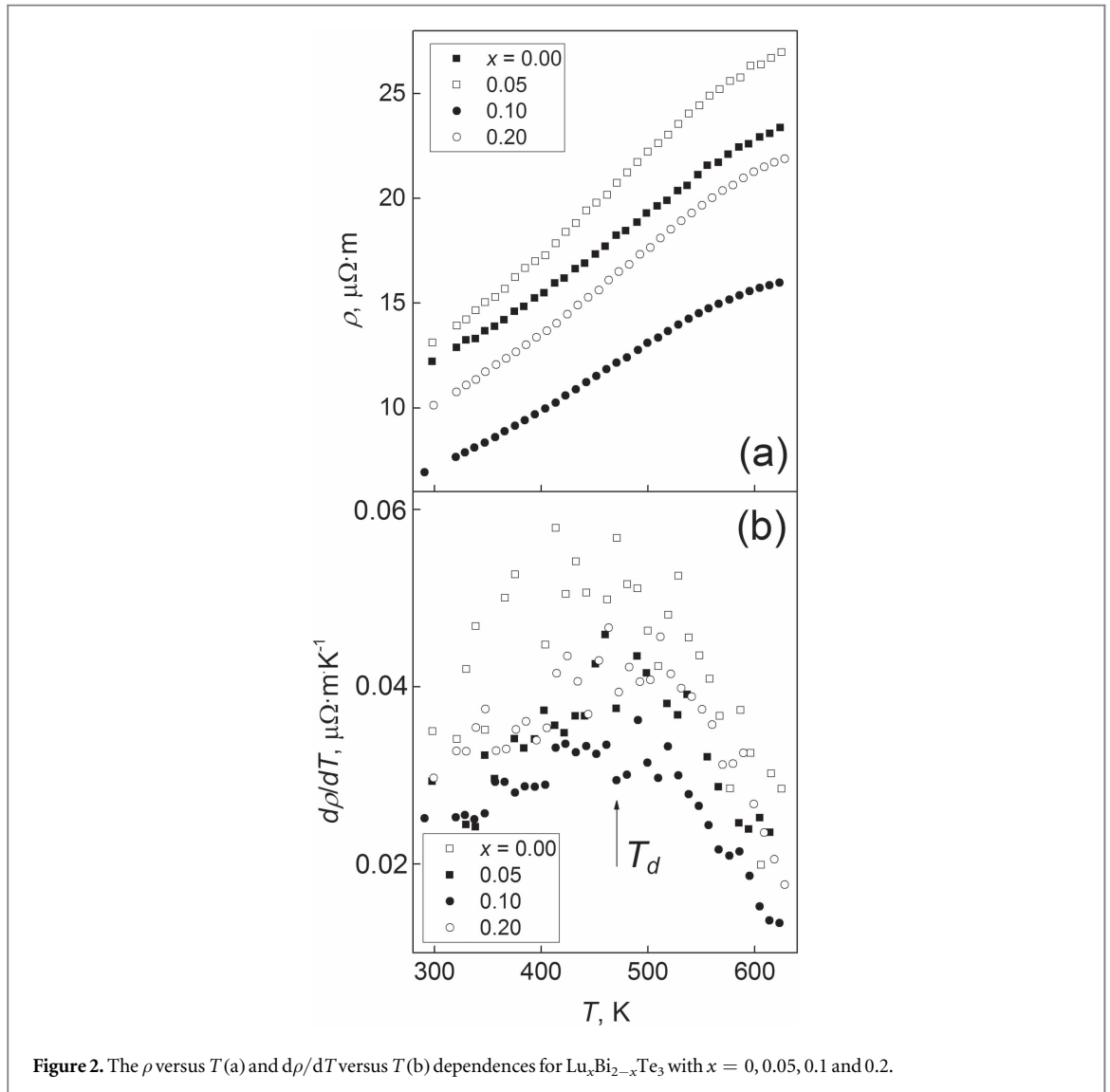
Figure 2. The ρ versus T (a) and dρ/dT versus T (b) dependences for Lu$_x$Bi$_{2-x}$Te$_3$ with $x = 0, 0.05, 0.1$ and 0.2.

Reducing the carrier mobility for Lu-doped Bi$_2$Te$_3$ can be related to alloying scattering of carriers [31, 32]. The alloy scattering is related to forming the point defects in the Bi$_2$Te$_3$ lattice as a result of substituting the Lu and Tm atoms for Bi site.

The specific electrical resistance

The temperature dependences of the specific electrical resistance for Lu$_x$Bi$_{2-x}$Te$_3$ with $x = 0, 0.05, 0.1$ and 0.2 are presented in figure 2(a). As is seen, first, ρ of all the compositions increases as temperature increases and, second, the $\rho(x)$ change is rather complicated. Further, to study the temperature behaviour of ρ in detail, the derivatives dρ/dT versus T were plotted in figure 2(b). Clear maximum is observed in the dρ/d$T(T)$ curves at temperature $T_d \approx 470$ K. This maximum can be related to a change of conductivity mechanism.

It is known that the specific electrical resistance of donor semiconductors is expressed as [21]

$$\rho = \frac{1}{e\mu n},\tag{4}$$

where μ is the electron mobility.

So, both $\rho(T)$ and $\rho(x)$ changes in figure 2(a) should be attributed to the corresponding changes of μ and n.

First of all, let us consider the temperature change of ρ. Bi_2Te_3 is known to be a degenerate semiconductor [33]. The degenerate semiconductors are characterized by the T-independent concentration of carriers. In this case, the temperature behaviour of ρ would be determined by the temperature behaviour of μ. For our experiments, the $\rho(T)$ behaviour at temperatures below T_d can be attributed to a regime of the degenerate semiconductor.

There are a few mechanisms determining the $\mu(T)$ dependence. Acoustic phonon scattering of carriers acting as main scattering mechanism at low temperatures results in the $\mu \sim T^{-3/2}$ dependence [34]. Above room temperature, acoustic and optical phonon scattering will be the dominant mechanism [35]. So, the $\mu \sim T^{-3/2}$ dependence is valid until a contribution of optical phonon scattering can be neglected. Above the Debye temperature, optical phonon scattering becomes comparable to acoustic phonon scattering and the temperature dependence of the carrier mobility can be described by an empirical expression given as

$$\mu \sim T^{-m},\tag{5}$$

with $1.5 < m < 2.5$.

For instance, the electron mobility for n-type silicon varies as $T^{-2.3}$ when both optical and acoustic phonon scattering become dominant.

According to figure 3(a), the best fit below T_d for the experimental $\rho(T)$ curves is corresponding to expression (5) with $m = -2.2$.

For high-temperature range above T_d, the $\rho(T)$ curves start to deviate from the $\rho(T) \sim T^{2.2}$ dependence. This deviation can be related to an onset of intrinsic conductivity. In this case, thermal excitation of the charge carriers from valence band to conduction band will generate both electrons in conduction band and holes in valence band decreasing ρ in accordance with expression (4). To distinguish an intrinsic conductivity contribution, $\Delta\rho(T)$, the experimental $\rho(T)$ curves should be subtracted from background $\rho(T) \sim T^{2.2}$ dependences shown as dashed lines in figure 3(a). The $\Delta\rho(T)$ dependences for $Lu_xBi_{2-x}Te_3$ with $x = 0, 0.05, 0.1$ and 0.2 are really the same for all the compositions. So, no noticeable doping effect on intrinsic conductivity of Bi_2Te_3 could be found in our experiments. It means that a band gap does not change at the doping.

Now, let us to analyse the $\rho(x)$ changes. As was mentioned above, both increase of n and decrease of μ_H take place as x increases (table 2). For the composition with $x = 0.05$, decrease of μ_H is a stronger effect compared to increase of n resulting in final increase of ρ at this doping level. So, the $\rho(T)$ curve for the composition with $x = 0.05$ is positioned above the $\rho(T)$ curve for undoped Bi_2Te_3. On the contrary, the $\rho(x)$ change for the composition with $x = 0.1$ will rather be determined by increase of n than decrease of μ_H. This composition has the lowest resistivity within whole temperature range under study. Finally, dominant source effecting on ρ for the composition with $x = 0.2$ will be again very strong decrease of μ_H. In this case, the $\rho(T)$ curve tends to the $\rho(T)$ curve for undoped Bi_2Te_3.

Further experiments should be done to account for the doping effect on both n and μ_H. However, it should be noted that this effect will be quite different for $n(x)$ and $\mu_H(x)$. Actually, Lu substituting for Bi or Te sites in the Bi_2Te_3 lattice works always as a scattering centre decreasing the carrier mobility. But, as was mentioned above (equation (2)), the antisite defects of Bi or Lu at Te sites should be produced to induce donor-like effect.

The Seebeck coefficient

The $S(T)$ dependences for $Lu_xBi_{2-x}Te_3$ with $x = 0, 0.05, 0.1$ and 0.2 are shown in figure 4(a). Since the majority charge carries are electrons, the Seebeck coefficient has a negative sign. The $S(T)$ curves have maximum typical for the Y-, Lu-, Ce-, Sm-doped Bi_2Te_3 compounds [21–23] and originated from a bipolar effect when two types of the charge carriers are present.

As a rule, thermal excitation of carries induced by intrinsic conductivity does not change the majority carrier concentration too much, but increases the minority carrier concentration. The Seebeck coefficient for electron conductivity is negative, whereas hole conductivity is characterized by the positive Seebeck coefficient. Competition of these two contributions with opposite signs of S will form the $S(T)$ maximum in figure 4(a).

It is known [21] that the Seebeck coefficient of the degenerate semiconductors can be expressed as

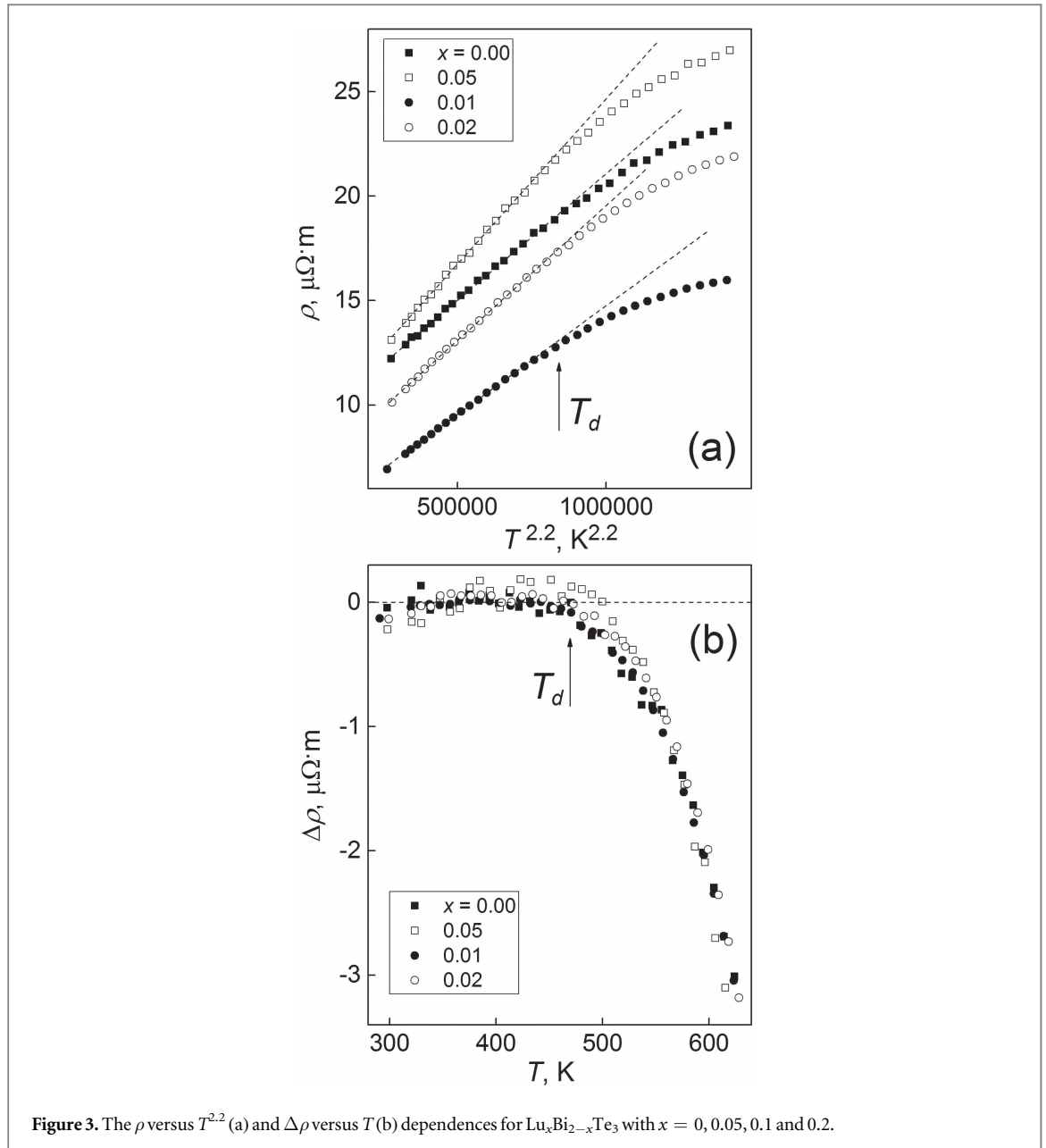$$S = \frac{2k_B^2 Tm^*}{3e\hbar^2}\left(\frac{\pi}{3n}\right)^{2/3}\left(\frac{3}{2} + \gamma\right),\tag{6}$$

Figure 3. The ρ versus $T^{2.2}$ (a) and $\Delta\rho$ versus T (b) dependences for $Lu_xBi_{2-x}Te_3$ with $x = 0, 0.05, 0.1$ and 0.2.

where k_B is the Boltzmann's constant, $\hbar$ is the reduced Planck constant, m^* is the density-of-state effective mass of electrons and γ is the scattering factor.

Expression (6) shows that the higher concentration of electrons decreases S, while the larger scattering factor increases the Seebeck coefficient. Normally, increase of ρ will be accompanied by increase of S. But, the $S(x)$ behaviour in figure 4(a) is more complicated and a clear S–x relationship cannot be found. So, the possible changes of m^* and γ in addition to the change of n should be taken into account to explain the $S(x)$ behaviour of Bi_2Te_3 at the doping. The value of γ is determined by mechanism of the charge carriers scattering. This mechanism is x-independent for all the compositions (figure 3(a)) and can be described by expression (5). So, the value of γ will be the same, too. It is known that γ is equal to $-1/2$ for acoustic phonon scattering and $1/2$ for optical phonon scattering [9]. As was discussed above, both optical and acoustic phonon scattering should be considered as dominant mechanisms to explain the $\rho(T)$ behaviour below T_d of the $Lu_xBi_{2-x}Te_3$ compounds with various x. Therefore, for further analysis of S, let us assume that $\gamma = -1/2$ (acoustic phonon scattering) $+ 1/2$ (optical phonon scattering) $= 0$. Next, in accordance with expression (6), the Seebeck coefficient should linearly be increased as T increases. As is shown by dashed lines in figure 4(a)), such kind of linear T-dependences of S are really observed within the temperature $290-370$ K range. Rate of the linear $S(T)$ growth can be characterized by a coefficient $\Delta S[\mu V\ K^{-1}]/\Delta T[K] \approx 2.14 \times 10^{-7}$. Using the values of n (table 2), $\Delta S/\Delta T$ and γ, the density-of-states effective mass of electrons can be estimated. The estimates of m^* are given in table 2 (m_0 is mass of free electron). So, at the doping m^* substantially increases from $0.11m_0$ for undoped Bi_2Te_3
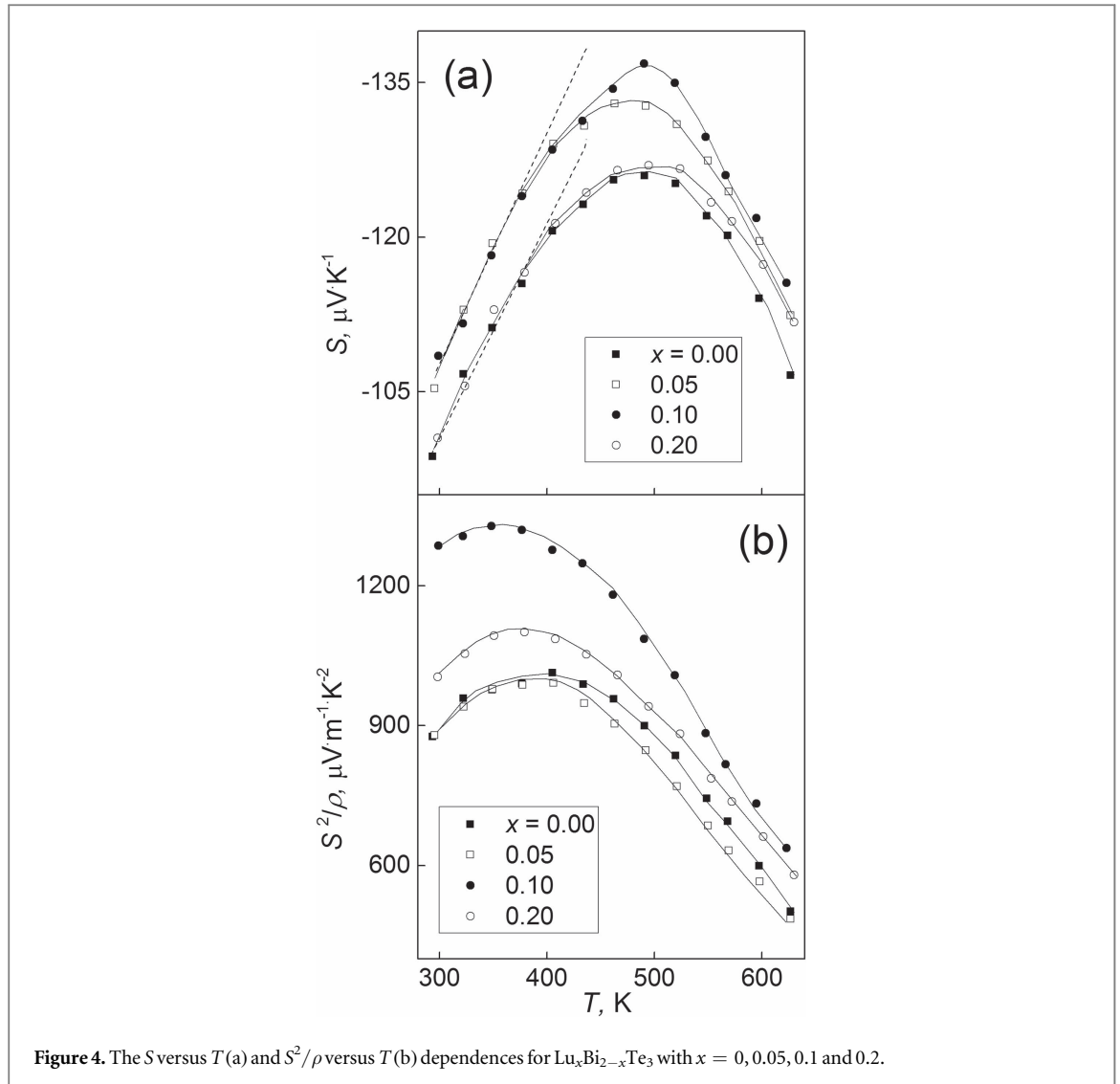
Figure 4. The S versus T (a) and S^2/ρ versus T (b) dependences for $Lu_xBi_{2-x}Te_3$ with $x = 0, 0.05, 0.1$ and 0.2.

up to $0.25m_0$ for $Lu_{0.2}Bi_{1.8}Te_3$. Increase of m^* can be related to forming the flat and narrow impurity band with high and sharp density of states near the Fermi level [36–38]. This doping effect was successfully used to explain the ZT improving in Tl-doped PbTe [39].

According to [38], the ideal electronic density of states to maximize the thermoelectric efficiency is the Dirac delta function. But, the ideal delta function is not achievable in real materials. However, electronic *f*-levels are tightly bound in atoms, and bind little in solids [40]. They give a sharp singularity in the density of states very near the Fermi level. This singularity is a Lorentzian of very narrow width. This is nature's closest approximation to the Dirac delta function. So, the impurity band originated from electronic 4*f*-levels of Lu can be characterized by sharp density of states near the Fermi level that results in increase of m^* and S in Lu-doped Bi_2Te_3.

Using the data in figures 2(a) and 4(a), the temperature dependences of the power factor, S^2/ρ, for $Lu_xBi_{2-x}Te_3$ with various x were plotted (figure 4(b)). These dependences combine the contributions from ρ and S. Due to the smallest ρ and highest S values, the power factor of the composition with $x = 0.1$ is much more compared to other compositions.

The thermal conductivity

The $k(T)$ dependences for Bi_2Te_3 and $Lu_{0.1}Bi_{1.9}Te_3$ are shown in figure 5(a). Thermal properties of these two compositions were analysed.

First, the total thermal conductivity of doped sample was observed to be substantially lower compared to pure Bi_2Te_3. Second, both $k(T)$ curves have a minimum related to a change of the thermal conductivity mechanism. The lattice (or phonon) thermal conductivity, k_p, electronic thermal conductivity, k_e, and bipolar thermal conductivity, k_b, should be taken into account to describe the thermal conductivity in this case.

The electronic thermal conductivity is related to the specific electrical conductivity, $\sigma = 1/\rho$, through the Wiedemann–Franz law [7]
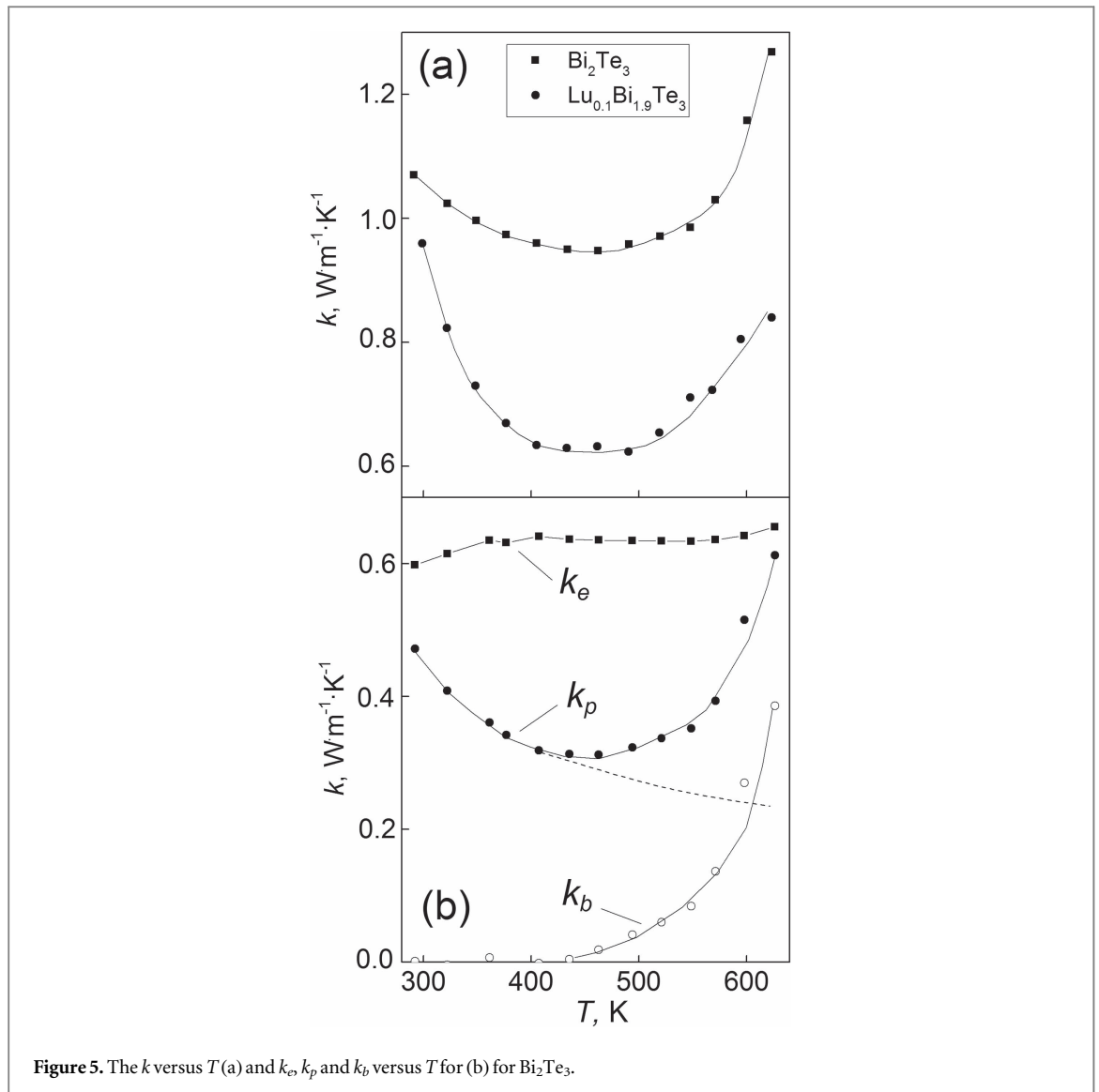
Figure 5. The k versus T (a) and k_e, k_p and k_b versus T for (b) for Bi_2Te_3.

$$k_e = L\sigma T, \tag{7}$$

where L is the Lorenz number.

The Wiedemann–Franz law was originally developed for metals and its use for semiconductors can be limited as it will be discussed later. For metals, the Lorenz number is a constant equal to $2.45 \times 10^{-8}\,\mathrm{W\Omega\,K^{-2}}$.

Nevertheless, although Bi_2Te_3 is a degenerate semiconductor, let us use the Wiedemann–Franz law to determine the electronic thermal conductivity. Then, the lattice contribution to the total thermal conductivity can be calculated as $k_p(T) = k(T) - k_e(T)$. But, in this case, the bipolar thermal conductivity will contribute at high temperatures (above the k_p minimum). Finally, the bipolar thermal conductivity contribution could be extracted. To do so, the $k_p(T)$ law must be defined. At high temperatures above the Debye, the lattice thermal conductivity usually decreases with increasing temperature as T^{-1} [41]. This is because, phonon specific heat is a constant at high temperatures in accordance with the Pettit–Delong law, and phonon energy increases linearly with temperature, i.e. the number of phonons increases linearly with temperature. As the scattering rate is proportional to the number of phonons, the thermal conductivity decreases with increasing temperature.

It was found that the experimental $k_p(T)$ dependence really obeys the $k_p \sim T^{-1}$ law. Then, the $k_b(T)$ contribution can be recovered by subtracting the phonon $k_p \sim T^{-1}$ background (a dashed line in figure 5(b)) from the experimental $k_p(T)$ curve above $k_p(T)$ minimum. When the bipolar thermal conductivity takes place, electron–hole pairs are thermally excited at hot-side of sample due to intrinsic conductivity process [42]. Then, these pairs as neutral formations move to cold-side. Finally, electron–hole pairs disappear due to a recombination process. The energy of recombination per one electron–hole pair equal or greater than the band gap will be emerged as a photon.

The contributions from k_e, k_p and k_b for Bi_2Te_3 are shown in figure 5(b). The electronic thermal conductivity seems to be anomalous high [43]. So, using the Lorenz number for metals results in incorrect estimate of k_e. It is
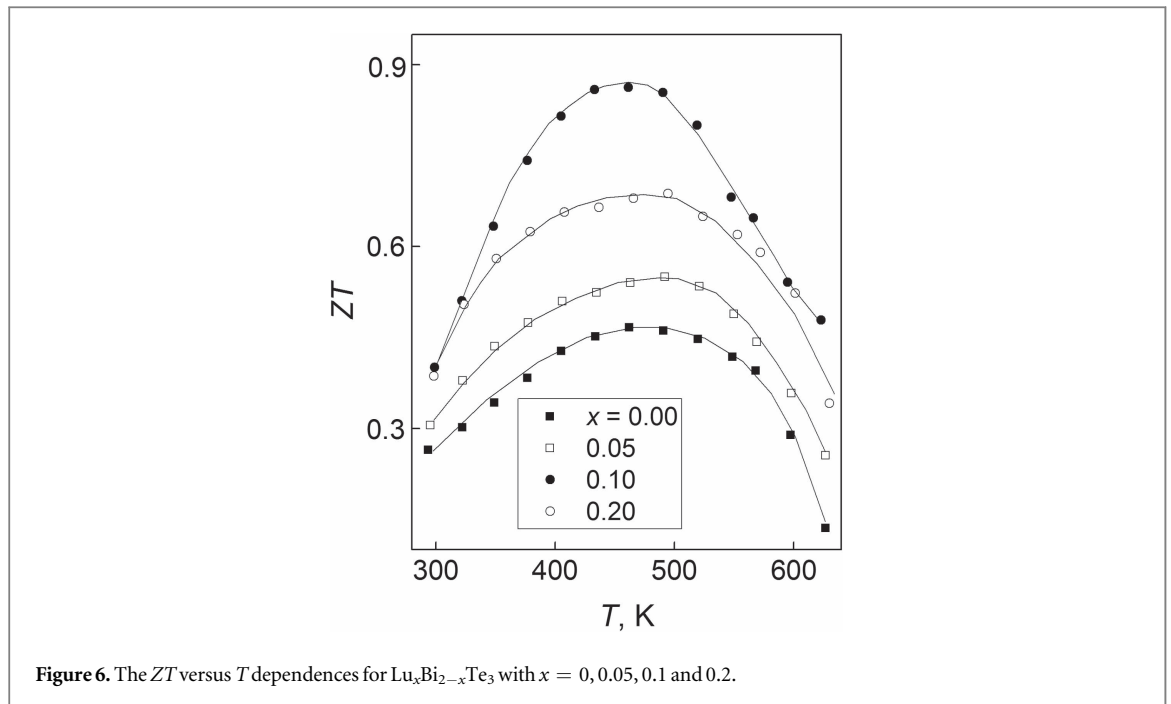
Figure 6. The *ZT* versus *T* dependences for $Lu_xBi_{2-x}Te_3$ with $x = 0, 0.05, 0.1$ and 0.2.

important to that the Wiedemann–Franz cannot correctly distinguish the contributions from k_e and k_p in many semiconductors, in which the Lorenz number depends on carrier density and electron scattering [44, 45].

Moreover, the Wiedemann–Franz calculation of the electronic and lattice thermal conductivities of $Lu_{0.1}Bi_{1.9}Te_3$ gives an unacceptable conclusion that the lattice thermal conductivity tends to zero, if the Lorenz number equal to 2.45×10^{-8} WΩ K^{-2} was assumed. So, the contributions from k_e, k_p and k_b cannot be determined for this composition.

Several mechanisms responsible for reducing the thermal conductivity of Bi_2Te_3 at the Lu doping could be considered. First, this doping can introduce a number of various point defects in the Bi_2Te_3 lattice like the antisite defects and Lu atoms substituting for the Bi sites. These defects can reduce k_e by scattering phonons due to either mass contrast or local strains. For instance, theoretically, k of Bi_2Te_3 can be decreased down to 20% by the antisite defects [46]. Second, besides the Lu doping effect on the lattice thermal conductivity, reducing the electronic thermal conductivity was theoretically predicted for semiconductors with narrow impurity band having high and sharp density of states near the Fermi level. Formation of such band originated from electronic 4f-levels of Lu was before assumed to explain the $S(x)$ behaviour (figure 4(a)). The physical reason for the reduce of k_e is that as the heat carried by an electron is proportional to the difference between its energy and the Fermi energy and materials with narrow density of states ($\Delta E/2$ less than several $k_B T$, where ΔE is width of band), which 'cut off' the high energy end of the Fermi distribution, have low k_e [37]. In this case, the Wiedemann– Franz law loses validity.

The thermal conductivity of Lu-doped Bi_2Te_3 with $x = 0.05$ and 0.2 also decreases compared to undoped compound. Again, the contributions from k_e, k_p and k_b cannot be defined by the Wiedemann–Franz law for these compositions.

Conclusion

Finally, the ρ, S and k values were used to plot the $ZT(T)$ dependences for $Lu_xBi_{2-x}Te_3$ with various x (figure 6). As is seen, the Lu doping results in remarkable increase of the thermoelectric figure-of-merit from $\sim$0.4 for undoped Bi_2Te_3 up to $\sim$0.9 for $Bi_{1.9}Lu_{0.1}Te_3$.

There are several mechanisms enhancing the thermoelectric efficiency of Bi_2Te_3 at the Lu doping. First of all, increase of the electron concentration reduces the specific electrical resistance. Then, formation of narrow non-parabolic impurity band with sharp density of states near the Fermi energy is believed to increase the Seebeck coefficient and decrease the electronic contribution to the total thermal conductivity. This impurity band can be originated from electronic 4f-levels of Lu. Besides, the antisite defects and Lu atoms substituting for Bi sites can also decrease the lattice thermal conductivity.

The onset of intrinsic conductivity observed above $T_d \approx 470$ K is harmful for the thermoelectric efficiency enhancement since thermal excitation of electron–hole pairs reduces the Seebeck coefficient and increases the thermal conductivity.

Acknowledgments

ORCID iDs

Oleg Ivanov ⓘ https://orcid.org/0000-0002-1803-5928

References

[1] Nolas G S, Sharp J and Goldsmid H 2001 *Thermoelectrics: Basic Principles and New Materials Developments* (New York: Springer) p 293
[2] Snyder G J and Toberer E S 2008 *Nat. Mater.* **7** 105
[3] Kitagawa H, Nagamori T, Tatsuta T, Kitamura T, Shinohara Y and Noda Y 2003 *Scr. Mater.* **49** 309
[4] Hyun D B, Oh T S, Hwang J S, Shim J D and Kolomoets N V 1998 *Scr. Mater.* **40** 49
[5] Miura S, Satob Y, Fukuda K, Nishimura K and Ikeda K 2000 *Mater. Sci. Eng.* A **277** 244
[6] Ivanov O, Maradudina O and Lyubushkin R 2014 *J. Alloys Compd.* **586** 679
[7] Liu W, Yan X, Chen G and Ren Z 2012 *Nano Energy* **1** 42
[8] Li Y, Jiang J, Xu G, Li W, Zhou L, Li Y and Cui P 2009 *J. Alloys Compd.* **480** 954
[9] Kim S S, Yamamoto S and Aizawa T 2004 *J. Alloys Compd.* **375** 107
[10] Morisaki Y, Araki H, Kitagawa H, Orihashi M, Hasezaki K and Kimura K 2005 *Mater. Trans.* **46** 2518
[11] Zhang Q, Che S, Liu W, Lukas K and Yan X 2012 *Nano Energy* **1** 183
[12] Mahan G, Sales B and Sharp J 1997 *Phys. Today* **50** 42
[13] Tritt T M 1999 *Science* **283** 804
[14] Lan Y C, Minnich A J, Chen G and Ren Z F 2010 *Adv. Funct. Mater.* **20** 357
[15] Duan X K, Hu K G, Ma D H, Zhang W N, Jiang Y Z and Guo S C 2015 *Rare Met.* **34** 770
[16] Srivastava P and Singh K 2014 *Mater. Lett.* **136** 337
[17] Jarivala B, Shah D and Ravindra N M 2015 *J. Electron. Mater.* **44** 1509
[18] Pan Y, Wei T R, Wu C F and Li J F 2015 *J. Mater. Chem.* C **3** 10583
[19] Hu L, Zhu T, Liu X and Zhao X 2014 *Adv. Funct. Mater.* **24** 5211
[20] Suh J *et al* 2015 *Adv. Mater.* **27** 3681
[21] Yang J, Wu F, Zhu Z, Yao L, Song H and Hu X 2015 *J. Alloys Compd.* **619** 401
[22] Ji X H, Zhao X B, Zhang Y H, Lu B H and Ni H L 2005 *J. Alloys Compd.* **387** 282
[23] Wu F, Song H, Jia J and Hu X 2013 *Prog. Nat. Sci. Mater. Int.* **23** 408
[24] Wu F, Shi W and Hu X 2015 *Electron. Mater. Lett.* **11** 127–32
[25] Ji X H, Zhao X B, Zhang Y H, Lu B H and Ni H L 2005 *Mater. Lett.* **59** 682
[26] Wu F, Song H Z, Jia J F, Gao F, Zhang Y J and Hu X 2013 *Phys. Status Solidi* a **210** 1183
[27] Shi W Y, Wu F, Wang K L, Yang J J, Song H Z and Hu X J 2014 *Electron. Mater.* **43** 3162
[28] Zhao X B, Zhang Y H and Ji X H 2004 *Inorg. Chem. Commun.* **7** 386
[29] Jia Y Q 1991 *J. Solid State Chem.* **95** 184
[30] El Kholdi M, Averous M, Charar S, Fau C, Brun G, Ghoumari-Bouanani H and Deportes J 1994 *Phys. Rev.* B **49** 1711
[31] Look D C, Lorance D K, Sizelove J R, Stutz C E, Evans K R and Whitson D W 1992 *J. Appl. Phys.* **71** 260
[32] Bennett H S 1996 *J. Appl. Phys.* **80** 3844
[33] Behnia K 2015 *Fundamentals of Thermoelectricity* (Oxford: Oxford University Press) p 256
[34] Kasap S, Koughia C, Ruda H and Johanson R 2006 *Handbook of Electronic and Photonic Materials* (Berlin: Springer) p 1407
[35] Neamen D A 2012 *Semiconductor Physics and Devices* (New York: McGraw-Hill) p 758
[36] Goldsmid H J 2012 *J. Electron. Mater.* **41** 2126
[37] Humphrey T E and Linke H 2005 *Phys. Rev. Lett.* **94** 096601
[38] Mahan G D and Sofo J O 1996 *Proc. Natl Acad. Sci. USA* **93** 7436
[39] Heremans J P, Jovovic V, Toberer E S, Saramat A, Kurosaki K, Charoenphakdee A, Yamanaka S and Snyder G J 2008 *Science* **321** 554
[40] Daybell M D and Steyert W A 1968 *Rev. Mod. Phys.* **40** 380
[41] Blakemore J S 1985 *Solid State Physics* 2nd edn (Cambridge: Cambridge University Press) p 520
[42] Wang S, Yang J, Toll T, Yang J, Zhang W and Tang X 2015 *Sci. Rep.* **5** 10136
[43] Chauhan D K, Notling W M, Poudeu P F P and Stokes K L 2015 *Mater. Sci. Semicond. Process.* **40** 453
[44] Tritt T M 2004 *Thermal Conductivity: Theory, Properties, and Applications* (New York: Plenum) p 285
[45] Bhandari C M and Rowe D M 1985 *J. Phys. D: Appl. Phys.* **18** 873
[46] Termentzidis K, Pokropyvnyy O, Woda M, Xiong S, Chumakov Y, Cortona P and Volz S 2013 *J. Appl. Phys.* **113** 013506